ELSEVIER

Infrared Physics & Technology 43 (2002) 101–107

INFRARED PHYSICS & TECHNOLOGY

www.elsevier.com/locate/infrared

Resonant enhancement of emission and absorption using frequency selective surfaces in the infrared

Irina Puscasu[a,*], William Schaich[b], Glenn D. Boreman[a,*]

[a] *School of Optics/CREOL, University of Central Florida, 4000 Central Florida Blvd., Orlando, FL 32816, USA*
[b] *Department of Physics, Indiana University, Bloomington, IN 47405, USA*

Received 12 September 2001

Abstract

We investigate the infrared properties of frequency selective surfaces consisting of aluminum patches on silicon substrates. Resonant behavior is found not only in the transmission and reflection, but also in the absorption and emission of these surfaces. The resonance location is a controllable function of the surface pattern. Simple model calculations reproduce well the qualitative behavior of our samples.

Keywords: Frequency selective surfaces; Absorption; Infrared

1. Introduction

The development of new sources in infrared spectroscopy for applications like selective and sensitive measurements of trace-gas concentrations [1–3] has received considerable interest. Typically, thermal sources of infrared radiation have a very broad spectral range and are massive and inefficient [4]. Semiconductor sources of IR radiation are narrow-band compact sources with high efficiency, but are limited to specific wavelengths and require complex fabrication processes.

Taking advantage of the evolution of the photolithographic manufacturing technology, alternative microstructured IR sources have been proposed. An array of free-standing metallic wires, thermally excited by an electric current, emits IR radiation in a narrow bandwidth, at wavelengths that depend on the dimensions of the structure [5]. Thermal emission from silicon machined lamellar gratings that support surface waves has also been studied [6,7].

In this work, we present a novel thermally excited source using an array of finite metallic elements on a dielectric substrate. Such structures are usually called frequency selective surfaces (FSSs) and have been used as filters in transmission or reflection [8–12]. The microconfiguration of the substrate's surface alters not only the transmission and reflection properties, but also the emission properties compared to those of a smooth surface, due to resonant interaction between the electromagnetic waves and the array. We demonstrate the approach by showing an enhancement of the

* Corresponding authors. Tel.: +1-407-823-6800; fax: +1-407-823-6880 (G.D. Boreman), +1-781-788-8811 (I. Puscasu).
E-mail addresses: ipuscasu@ion-optics.com (I. Puscasu), boreman@creol.ucf.edu (G.D. Boreman).

1350-4495/02/$ - see front matter
PII: S1350-4495(01)00134-7

emitted radiation at the specific wavelength of 5 μm, which falls in one of the spectral ranges where water vapor in the atmosphere absorbs. By increasing the emission of the thermal source in this particular spectral range, one can increase the capability of such a source to probe through the atmosphere, or alternatively to mask the thermal emission of a surface by emphasizing the emitted power in the region where the atmosphere is opaque. Depending upon the application, the resonant wavelength can be tuned by changing the array design parameters.

Absorption in FSSs due to either ohmic or dielectric losses has been usually neglected, FSSs being treated in the perfect conductor limit, on lossless substrates. In this paper, we consider FSSs that consist of rectangular arrays of thin aluminum (Al) dipoles or cross patches mounted on silicon (Si) substrates. Significant losses occur in both the arrays and the substrate. Our goal is to exhibit the resonance in absorption of such structures and to show that the same parameters control the location and shape of the resonance for transmission, reflection, absorption and emission. To our knowledge, a comparative study between theory and experiment of the absorptive and radiative properties of an infrared FSS has not been carried out before in this infrared spectral band.

2. Fabrication

The fabrication of the microstructured surfaces was performed using the Cornell Nanofabrication Facility located at Cornell University. The Si substrates have been n-doped, with a thickness of 380 μm and a dc resistivity of $\approx 5\ \Omega\,\mathrm{cm}$. Arrays of Al dipoles or crosses of total extent $5 \times 5\ \mathrm{mm}^2$ have been fabricated by direct-write e-beam lithography, using a double layer resist lift-off metalization technique [13] that takes advantage of the large undercut to write very small features. The two-layer PMMA/P(MMA–MAA) copolymer resist was exposed by a focused electron beam using the Cambridge Instruments EBMF-2 electron beam pattern generator. The dose that resulted in the highest quality exposures was about 480 $\mu\mathrm{C}/\mathrm{cm}^2$. The two-layer resist was then developed in a 1:3 solution of methyl isobutyl ketone and isopropanol. A thin film of Al was deposited on the substrate. Removal of the unexposed resist was accomplished by tape-assisted lift off followed by a submerging of the metalized substrate in methylene chloride, accompanied by an ultrasound-assisted agitation.

Fig. 1 shows three scanning electron micrographs of an isolated-dipole, a coupled-dipole and a cross array supported by a Si substrate. The metallic features in all cases are about 30 nm thick. The geometrical parameters needed for model calculations have been labeled. Both the element size and periodicity must be specified. Their measured values for the arrays studied in this paper are listed in Table 1.

3. Spectral reflection and transmission

In order to characterize the spectral response of the arrays, we performed Fourier transform spectroscopy. The spectral data were taken on a Perkin-Elmer 1710 infrared Fourier transform spectrometer with the spectral resolution set to 4 cm^{-1}. The weak intensity of the source over the short wavelengths between 3 and 4 μm caused some data corruption by an increased noise level. Further, although the atmosphere in the FTIR chamber was controlled by a continuous flow of nitrogen gas, we still noticed some measurement errors near strong water absorption lines. Fig. 2a shows results for a coupled-dipole array that resonates near 5 μm. We call the region of the substrate covered by the metal array the active area, while any uncovered region is called the inactive area. The transmission and reflection coefficients for active (inactive) areas are denoted by T and R (T_0 and R_0). In Fig. 2a we plot the relative quantities T/T_0 and R/R_0 which emphasize the resonant behavior. The absorption observed between 8 and 9 μm is caused by a strong lattice vibration of Si–O, due to the oxygen occluded during the crystal growth or due to the oxidation of the substrate surface in contact with the atmosphere [14].

To help understand the spectral response of our FSS we have used a simple simulation code. The details of the mathematical model, including its

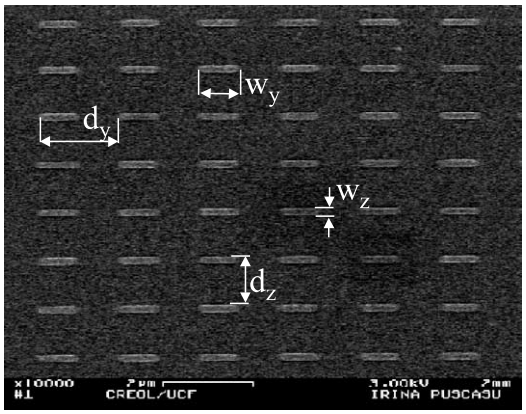

a)isolated-dipole array

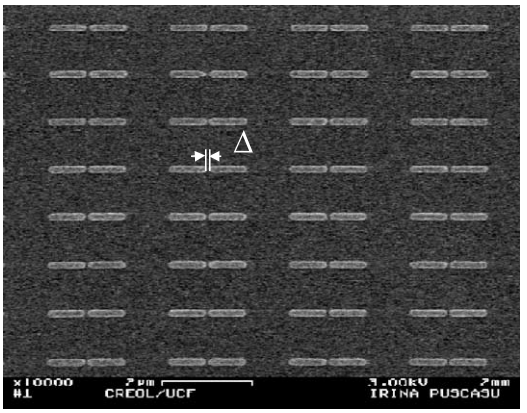

b) coupled-dipole array

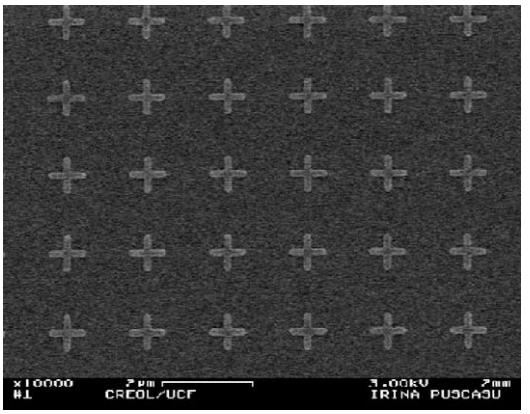

c) cross array

Fig. 1. Scanning electron micrographs of several patch arrays. The values of the geometrical parameters are in Table 1, samples A3, A1, A6 correspond to parts a, b, c, respectively. The element spacing within a unit cell for part b, $\Delta = 0.074$ μm.

parameterization and solution, have been described before [15] and we follow basically that procedure here. The metal elements of the FSS are described with a complex-valued, frequency-dependent sheet resistance and the current is allowed to flow solely along the long axis of an element with no variation across the narrow width of the structure.

In Ref. [15] the substrate was approximated as lossless and only the transmission into the substrate was calculated. Here we have included losses and multiple reflections within the substrate. However the $D = 380$ μm thickness of the substrate leads to Fabry–Perot oscillations too rapid to be resolved, so we can neglect the phase of the radiation. The net transmission is then described by

$$T = \hat{T}_1 \Gamma T_1 / [1 - \Gamma^2 \hat{R}_{1s} R_1] \quad (1)$$

where $\Gamma = |\exp(2ik_s D)|$ with $k_s = (\omega/c)\sqrt{\varepsilon_s}$. Here ω is the light's frequency, ε_s the substrate dielectric function and quantities with a caret are for the interface with the FSS. For an inactive area $\hat{T}_1 \to T_1$ and $\hat{R}_{1s} \to R_1$, the transmission and reflection coefficients of a vacuum/Si interface. $\hat{R}_{1s}$ is the reflection coefficient for a beam incident from within the substrate on the interface with the FSS. We write $\varepsilon_s = \varepsilon_b + i\sigma_s/(\omega\varepsilon_0)$ with $\varepsilon_b = 11.7$ and the conductivity σ_s chosen to fit the measured absorption of roughly 0.01 for inactive areas (at least for wavelengths below 8 μm). This leads to the constant value $\sigma_s = (400\ \Omega\text{cm})^{-1}$. The losses parameterized by σ_s only appear in ε_s and Γ; we calculate T_1 and R_1 with σ_s set to zero, yielding the frequency-independent values $T_1 = 0.70$ and $R_1 = 0.30$. The result for Γ is also essentially independent of frequency since for small σ_s, $\text{Im}\sqrt{\varepsilon_s} \approx \sigma_s/(2\varepsilon_0\omega\sqrt{\varepsilon_b})$ and $\Gamma \approx \exp(-\sigma_s D/(c\varepsilon_0\sqrt{\varepsilon_b})) = 0.99$.

In our calculations of $\hat{T}_1$s and $\hat{R}_1$s, we consider only the energy carried by beams moving along the surface normal. For the parameters of our systems, diffraction effects are in general weak. Even if a diffraction event switches the incident beam from moving normal to the surface in vacuum to moving obliquely within the Si, the internal beam cannot generally refract back into vacuum due to total internal reflection. A second diffraction event is required for escape. Thus a single diffraction

Table 1
Array characteristics

Array label	Array type	w_y (μm)	w_z (μm)	d_y (μm)	d_z (μm)
A1	Coupled dipole	0.832	0.152	2.702	1.087
A2	Isolated dipole	1.71	0.161	2.690	1.077
A3	Isolated dipole	0.847	0.171	1.845	1.138
A5	Cross	1.82	0.176	2.808	2.840
A6	Cross	0.81	0.148	1.810	1.805

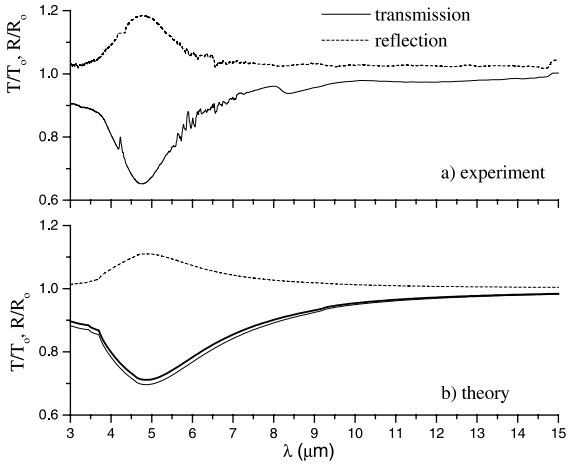

Fig. 2. Relative transmission and reflection through sample A1 (see Fig. 1b) versus vacuum wavelength. The thinner line for the theoretical T/T_0 is from the scheme of Ref. [15].

effectively traps the light inside the Si and contributes to the system absorption. Hence if two (or more) diffraction events are negligible, our calculational scheme should be reasonable.

The analog of Eq. (1) for the net reflection is

$$R = \hat{R}_{1v} + \hat{T}_1 R_1 \Gamma^2 \hat{T}_1 / (1 - \Gamma^2 \hat{R}_{1s} R_1) \quad (2)$$

where the only new quantity, $\hat{R}_{1v}$, is the reflection coefficient for the FSS when the incident beam comes from vacuum. When there are losses in the metal elements of the FSS, $\hat{R}_{1v} \neq \hat{R}_{1s}$, but both become R_1 over inactive areas. Fig. 2b illustrates calculated relative transmission and reflection coefficients for the coupled-dipole array whose measured response is shown in Fig. 2a. For these (and all later calculations) the Al sheet resistance is taken as $(9 + i10/\lambda)$ Ω/sq where λ is in μm. Although experiment and theory differ in fine quantitative details, the qualitative agreement is good. The resonance arises from a standing wave of current along the long axis of an element, with nodes at each end and an antinode in the center.

In Ref. [15] our analysis ignored the multiple scattering of the light within the substrate. This led in the present notation to $T/T_0 = \hat{T}_1/T_1$ instead of the result implied by Eq. (1), $T/T_0 = (\hat{T}_1/T_1) \times [1 - \Gamma^2 R_1^2]/[1 - \Gamma^2 \hat{R}_{1s} R_1]$. Both of these expressions are plotted in Fig. 2b and are quite similar.

4. Spectral absorption and emission

The radiative properties of a surface are closely related to its structure. This dependence can be used to modify the radiative properties. The presence of an array of metallic elements with dimensions smaller than the wavelength can increase the emission from a surface in a resonant way. To show this, spectral emission measurements were performed using a Graseby radiometer. The sample is in contact with an aluminum hot plate, held at a temperature of 170 °C. A set of two apertures is used to assure that the radiometer collects only the radiation from the desired small area on the Si wafer, due to the fact that the footprint of the detector in the object plane is bigger than the dimensions of the FSS. To decrease the concentration of the water vapor and carbon dioxide in the atmosphere, an aluminum tube was inserted between the radiometer and the aperture set. With a continuous flow of nitrogen gas through the pipe, the detector signal between 3 and 15 μm was considerably increased and the signal to noise ratio improved.

In Fig. 3 we present radiance measurements from the active and inactive area on the Si wafer for a coupled-dipole FSS (array A1). A blackbody

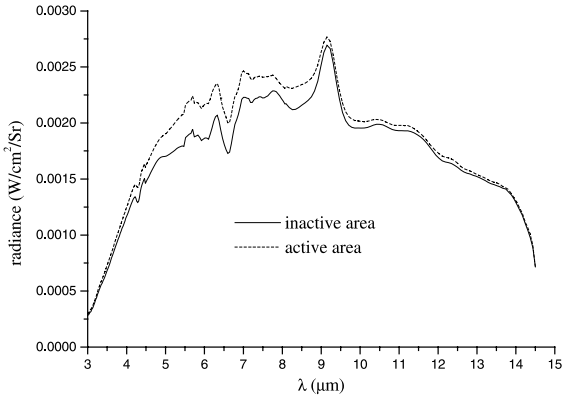

Fig. 3. Measured radiance versus vacuum wavelength for the active and inactive areas of sample A1 of coupled dipoles.

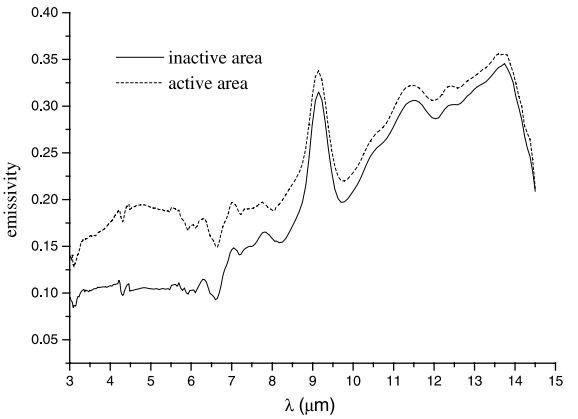

Fig. 4. Measured emissivity versus vacuum wavelength for active and inactive areas of sample A1.

was used for calibration purposes. One can discern a resonant enhancement.

To obtain a plot for the spectral emissivity we must account for the fact that the Si substrate is transparent at the wavelengths of interest. There are three phenomena taking place: the samples transmit radiation coming from the hot plate, they also emit radiation due to their elevated temperature and finally they reflect the background radiation. So, we define the emissivity of the samples along the surface normal for each wavelength as follows:

$$\varepsilon_s = \frac{L_s - T_s L_{hp} - R_s L'_{bkg}}{L_{bb}} \tag{3}$$

Here L_s and L_{hp} represent the measured radiance of the sample and hot plate, respectively at the elevated temperature of 170 °C; L'_{bkg} is the measured radiance of the background that is at the room temperature of 22 °C; T_s and R_s represent the transmission and reflection, respectively of the sample; and L_{bb} is the radiance of a blackbody at 170 °C. In Fig. 4 we present the spectral emissivity for the active and inactive area on the Si wafer for the coupled-dipole array. To produce these curves we replaced the T_s and R_s in Eq. (3), with T'_s and R'_s, our measured values at room temperature. Although the values of the transmission and reflection coefficients probably change by several percent between 22 and 170 °C, these differences should not qualitatively distort the plotted ε_s.

Emission and absorption of radiation are related processes. Indeed Kirchhoff's law [16] states that the spectral emissivity ε equals the spectral absorption a under the same conditions. We are interested in the change in absorption and/or emission that is introduced (Δa or $\Delta\varepsilon$) by the periodic structures placed on the Si substrate. We define the emissivity change as the difference between the emissivity ε_{FSS} of the FSS on the Si substrate heated to an elevated temperature, and the emissivity ε_{Si} of the substrate alone at that temperature

$$\Delta\varepsilon = \varepsilon_{FSS} - \varepsilon_{Si} \tag{4}$$

We will compare $\Delta\varepsilon$ with the extra absorption $\Delta a'$, which represents a similar difference taken between the absorption of the FSS on the Si substrate,

$$a'_{FSS} = 1 - T'_{FSS} - R'_{FSS} \tag{5}$$

and the absorption of the clean Si substrate,

$$a'_{Si} = 1 - T'_{Si} - R'_{Si} \tag{6}$$

so

$$\Delta a' = a'_{FSS} - a'_{Si} \tag{7}$$

Primes appear in Eqs. (5)–(7) because the reflection and transmission measurements were only performed with the samples at room temperature. To the extent that the absorption due to the substrate Si and the overlayer FSS are independent, one expects that $\Delta a' \approx \Delta a$ and hence that $\Delta a' \approx \Delta\varepsilon$.

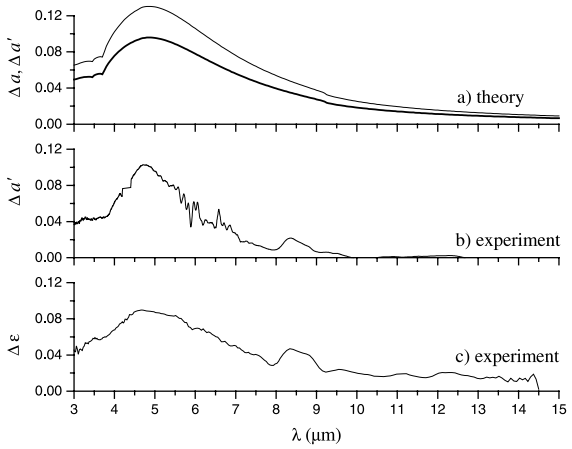

Fig. 5. Extra emission and absorption versus vacuum wavelength for the coupled-dipole sample A1. The primed (unprimed) quantities are determined primarily by quantities at room (elevated) temperature. For the theoretical curves the thicker (thinner) curve is Δa ($\Delta a'$).

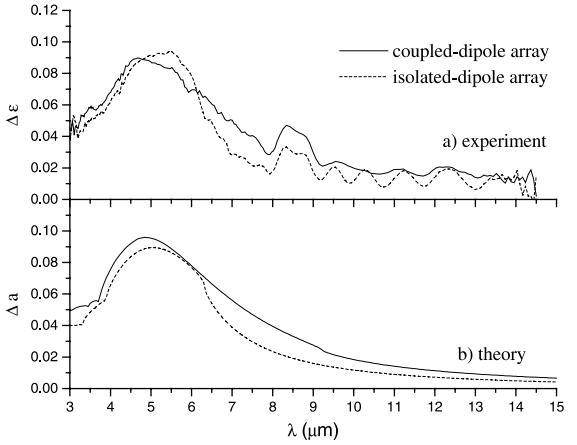

Fig. 6. Extra emission or absorption versus vacuum wavelength for the samples A1 and A3.

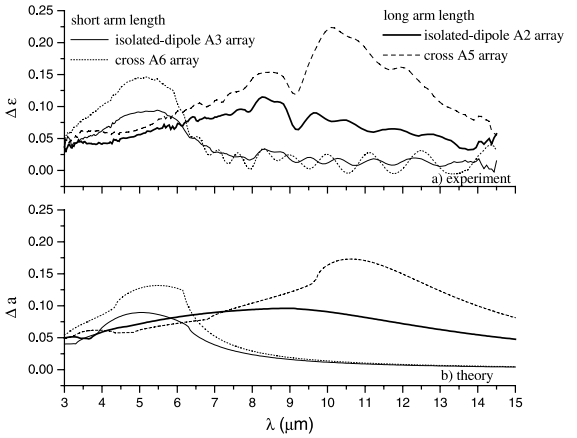

Fig. 7. Extra emission or absorption versus vacuum wavelength for the samples A2, A3, A5, A6.

In Fig. 5 we present the extra absorption measured and calculated and the measured extra emission. The calculations were done in two ways. We used first the value of $\sigma_s = (400\ \Omega\text{cm})^{-1}$ fitted to the room temperature measurements of T_s', R_s' to find $\Delta a'$ as defined in Eq. (7). Then we increased the frequency-independent σ_s to $(36\ \Omega\text{cm})^{-1}$ in order to produce an $a_{Si} \approx 0.10$. The idea is that this increased substrate conductivity represents the effect of raising the temperature to 170 °C—see the inactive curve in Fig. 4. With this new choice of σ_s we then calculated Δa from Eqs. (5)–(7) without primes. The only qualitative difference between the two theoretical results appears in the overall strength, with $\Delta a' > \Delta a$. Just as in Fig. 2 there is an enhancement centered at 5 μm. On resonance there is an increased magnitude of the induced current oscillating in each metal patch. This leads to an enhanced absorption of the FSS through Joule heating. There is a good agreement between theory and experiment for the absorptive and radiative properties of the FSS.

In Fig. 6 we compare the spectral response of the isolated-dipole versus coupled-dipole arrays with comparable sized elements. The surprising feature of the data is that the close coupling of patches only slightly changes the resonance locations [12,15]. Again the theory qualitatively reproduces the experimental structures.

Finally in Fig. 7 we compare the spectral response of two sets of isolated-dipole or cross arrays. The samples with cross arrays on the surface exhibit a larger enhancement compared to the samples with dipole arrays due to an increased filling factor and also due to the different element shape. The samples with dipole arrays react resonantly only to the radiation that is polarized parallel to the length of the dipoles. The radiation

with polarization perpendicular to this dimension will pass through or be emitted unperturbed. The dipole array samples could hence be used in applications involving polarized radiation. For the cross array samples, both orthogonal polarizations will interact resonantly with the array, producing a larger increase of the radiation emitted in the resonant spectral range. In the model calculations for the cross arrays we treat the two arms of each cross independently. The different polarizations produce the (same) resonance in the different arms. This simple treatment appears to be adequate. In Fig. 7 we also observe the shift in the wavelength of resonance for the emitted radiation from ≈ 5 to 11.5 μm as we increase the length of the dipole or cross arm from 0.8 to 1.8 μm.

5. Conclusions

In general, the absorption of FSSs has been neglected. The microconfiguration of the substrate's surface also alters resonantly the absorption and emission properties compared to those of the inactive surface. We demonstrate an enhancement of the emitted radiation centered at specific wavelengths in the 3–15 μm region. Depending upon the application, the resonant wavelength can be tuned by proper choice of the array design parameters. The enhancement of surface emission should find applications in the development of new sources for infrared spectroscopy, or in IR signature management.

Acknowledgements

Some of the calculations were done using the computer resources provided by the National Partnership for Advanced Computational Infrastructure at the San Diego Computer Center.

References

[1] S.D. Smith, A. Vass, P. Bramley, J.G. Crowder, C.H. Wang, Comparison of IR LED gas sensors with thermal sources products, IEE Proc. Optoelectron. 114 (1997) 266–270.
[2] J. Meneses, F. Lopez, J. Melendez, A.J. de Castro, S. Bosch, Fabry–Perot resonators for high-resolution infrared gas sensors, Proc. SPIE 2776 (1996) 279–290.
[3] J. Melendez, A.J. de Castro, F. Lopez, J. Meneses, Spectrally selective gas cell for electrooptical infrared compact multigas sensor, Sens. Actuat. A: Phys. 47 (1995) 417–421.
[4] M.A. Bramson, Infrared Radiation, Plenum, New York, 1968.
[5] S.O.C. Giraud, D.G. Hasko, Mesoscale thermal infrared sources, Microelectron. Engng. 41/42 (1998) 579–582.
[6] P.J. Hesketh, B. Gebhart, J.N. Zemel, Measurements of the spectral and directional emission from microgrooved silicon surfaces, J. Heat Transfer Trans. ASME 110 (1988) 680–686.
[7] J. Le Gall, M. Olivier, J.J. Greffet, Experimental and theoretical study of reflection and coherent thermal emission by a SiC grating supporting a surface-phonon polariton, Phys. Rev. B 55 (1997) 10105–10114.
[8] R. Ulrich, Far infrared properties of metallic mesh and its complementary structure, Infrared Phys. 7 (1967) 37–55.
[9] E.L. Pelton, B.A. Munk, Scattering from periodic arrays of crossed dipoles, IEEE Trans. Antenn. Propag AP-27 (1979) 323–330.
[10] C.M. Rhoades, E.K. Damon, B.A. Munk, Mid-infrared filters using conducting elements, Appl. Opt. 21 (1982) 2814–2816.
[11] D.M. Byrne, A.J. Brouns, F.C. Case, R.C. Tiberio, B.L. Whitehead, E.D. Wolf, Infrared mesh filters fabricated by electron-beam lithography, J. Vac. Sci. Technol. B 3 (1985) 268–271.
[12] I. Puscasu, D. Spencer, G. Boreman, Refractive-index and element-spacing effects on the spectral behavior of infrared frequency-selective surfaces, Appl. Opt. 39 (2000) 1570–1574.
[13] Y. Todokoro, Double-layer resist-films for optical and electron beam microlithography, Trans. Ins. Electron. Commun. Eng. Jpn. Sect E (Engl) E65 (1982) 23–27.
[14] T. Sato, Spectral emissivity of silicon, Jpn. J. Appl. Phys. 6 (1967) 339–347.
[15] I. Puscasu, W.L. Schaich, G.D. Boreman, Modeling parameters for the spectral behavior of infrared frequency-selective surfaces, Appl. Opt. 40 (2001) 118–124.
[16] W.L. Wolfe, Introduction to Radiometry, vol. TT29, SPIE Press, Bellingham, WA, 1998.